

INVESTIGATION THE EFFECT MIXING GRAIN SIZE AND EPOXY GLUE CONTENT ON INDEX PROPERTIES OF SYNTHETIC SANDSTONE SAMPLE

Ekhwaiter Abobaker¹, Abadelhalim Elsanoose¹, Mohammad Azizur Rahman², Amer Aborig¹, Yan Zhang¹, Edison Sripal¹

¹Memorial University of Newfoundland, St. John's, NL, Canada

²Texas A&M University at Qatar, Doha, Qatar

Abstract: Evaluating petroleum reserves requires an initial investigation of the relevant petrophysical characteristics of a target area's sandstones. In general, the most common type of host rocks represented in the hydrocarbon reservoirs are sedimentary rocks, which includes sandstone. This paper presents a technique for preparing four homogenised synthetic sandstone samples that can be applied in the hydrocarbon recovery projects. The approach mixes sand together with epoxy glue and can be employed in the evaluation of synthetic sand plug characteristics and then compared with fine-grained sandstone sample. The study conducted extensive laboratory testing using lab-created synthetic sandstone samples of four sandstone grain sizes. The three synthetic sandstone samples were made from four different sandstone grain sizes, and one sample was a mixture of two different grain size with various amount of epoxy. Mercury intrusion porosimetry (MIP) and scanning electron microscopy (SEM) have been used to first characterize and then analyze the pore morphology and index properties for the synthetic samples. The index properties included permeability, porosity, median pore diameter, tortuosity, and pore size distribution. The experimental results indicated that weak solidified sandstone index characteristics are strongly affected by both mixing and grain size. In addition, SEM map images revealing pore morphologies and homogenised grain distribution of the tested samples indicate that grains that undergo reductions in size require additional epoxy glue content, likely due to binder distribution of glue among the small grains.

Keywords-component; synthetic sandstone sample; mixing grain size ; epoxy glue content

Introduction

Investigations into the properties of reservoirs necessitates the study of the surrounding rock formations to be done quantitatively. As a sedimentary rock class, sandstones are well-known as typical host rocks in the hydrocarbon

reservoirs, so the characteristics of sandstones have a significant impact on the development and success of drilling projects. Accordingly, it is important to understand the characteristics not only of sandstones but of their interrelationships with the immediate drilling environment. We can assert that the characteristics of sandstone hold economic significance, which means that knowledge about these characteristics is needed to determine a reservoir's potential and capacity in hydrocarbon production.

Over the years, enhanced oil recovery (EOR) experiments have been performed at various oil laboratories using different kinds of rocks commonly found in reservoir areas. These rocks include but are not limited to Botucatu, limestone and Berea sandstones (Cardoso & Balaban, 2015) [1]. As sourcing natural samples can be both expensive and challenging, and because these samples, if found, are often anisotropic (i.e., display various characteristics depending on how they are analyzed), labs tend to rely on models (Marques et al., 2011 [2]; Fattahpour et al., 2014 [3]). To develop a pore model, the topology and geometry must be known, along with the properties of the pore space. As explained by Xiong et al. in [4], finding the properties of pore space usually involves the use of mercury intrusion porosimetry, gas adsorption, and direct imaging. These researchers also looked at development methods for primary pore networks. Furthermore, Xiong et al. found that pore network models can be invaluable tools in the prediction of mesoscale phenomena such as the linking of single pore processes [4]. The current state of the technique uses mercury intrusion porosimetry (MIP) and scanning electron microscopy (SEM) for analyzing the main index characteristics and pore morphologies in sandstones that are weakly solidified. Both MIP and SEM are employed in the quantitative and qualitative assessments of pore structural features in various types of rock samples. In the hydrocarbon field, SEM-based imaging techniques have typically been employed to visually characterize pore systems of reservoir rocks at the nanoscale. We will look at recent SEM-related

studies first. Yang et al. [5] and Sun et al. [6] applied high-resolution FE-SEM techniques to study nanoscale pore features in organic-rich Wufeng-Longmaxi shale and the Lower Cambrian Niutitang shale, respectively. Loucks et al. [7] also used SEM and FE-SEM to examine and analyze pore type as well as lithologic composition in shale and mudstone. Klaver et al. [8] employed BIB-SEM and focused on pore space morphology for their Posidonia shale study. In related work, Jiao et al. [9] and Zhou et al. [10] used FIB-SEM to explore 2D and 3D nano pore properties, respectively, in Longmaxi gas shales.

In MIP, the features of pore structure are examined more indirectly, providing a broader overview of pore information such as porosity, distribution, and permeability. MIP, which has been used for decades in various industries, utilizes capillary pressure measurements to characterize pore structure in a variety of porous media [11, 12]. The main advantages of using the MIP technique are that it is time-saving, easy to operate, and features wide pore-throat sizes that typically measure from 3 nm to 250 μm . Numerous researchers have investigated the pore structure for different reservoir rocks using MIP. In [13], Zhang et al. used data from MIP measurements to examine pore structure properties and permeability in several different deep sedimentary rocks, including sandstone, coarse sandstone, medium sandstone, fine sandstone, siltstone, mudstone, sandy mudstone, and conglomerate. Yang et al. [14] looked at the various qualities in pore systems of Longmaxi shales and organic-rich Wufeng by applying a few complementary strategies along with MIP. In [15], Lai and Wang explored pore fractal features prevalent in tight gas sandstones by employing high-pressure mercury intrusion methods.

In acknowledgement of previous work done in the field, the present study seeks to obtain homogenised synthetic sandstone samples from mixing sand and epoxy glue to be used potentially in EOR studies. It also looks to further explore and define microscale pore structure characteristics, along with the porosity and permeability of synthetic samples, utilizing both SEM and MIP in combination. These findings will then serve as a basis of comparison with natural fine-grained sandstone samples that are typically utilized for enhanced oil recovery (EOR).

I. EXPERIMENTAL METHODS

A. Sample preparation

In the laboratory experiments, four highly permeable synthetic sandstone samples undergo preparation. The four cylindrical samples were made of sand particle measuring 0.18 to 1.18 mm as shown in Fig. 1. To begin the preparations and experiments, sieve analysis is conducted in order to quantitatively gauge the size of the sandstone samples' grains or particles. The aggregate samples are then dried inside a hot-air oven (thermostatically controlled) at temperatures between 105° C and 110° C. The samples are oven-dried for 24 hours and then sieved. Following the sieving, an analysis is conducted for an aggregate sample, with the sample obtained after using a 1.18 mm and smaller sieve net. The synthetic

sandstone samples have been created using sandstones of various sizes or by mixing two different sizes in the 0.18 mm to 1.18 mm range after sieving using epoxy glue. The sandstone and epoxy glue were mixed in different quantities (depending on the size of the sand) by using an electric mixer for 10 minutes. The mixture is then placed in a plastic container over the course of four different stages, using an electric vibrator to ensure the distribution of grain with epoxy glue.



Fig. 1. THE FINE-GRAINED AND FOUR SYNTHETIC SAMPLES

The samples measure 12 inches high (H), with a radius (D) of 6 inches and the hole (d) in the center of the sample 0.50 inch (at the center-point of the diameter) as explained in Fig. 2. Initially, the samples were created without a hole (P_d) in the center of the sample. Then, a hole was made in the middle of the sample measuring 0.5 inches (radius) by 10 inches (depth).

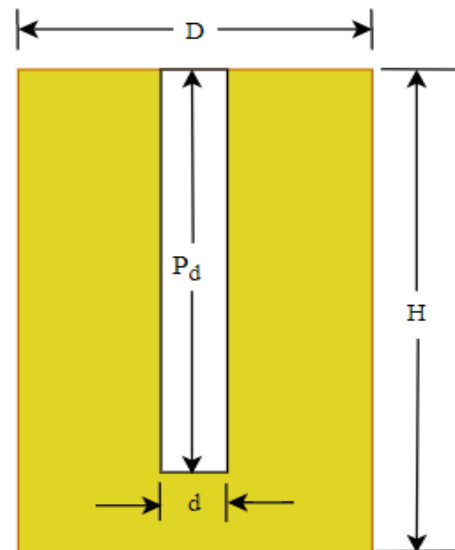


Fig. 2. THE DIMENSIONS OF SANDSTONE SAMPLE.

The large samples will be used to study the multiphase flow in the porous media, and the cores taken from the large

samples are used in this study to obtain petrophysical properties of the samples. The weight of the sand and the amount of epoxy glue in each sample is presented in Table 1.

TABLE I. SAMPLE PREPARATION DETAILS.

Sample name	The weight of the sand and the amount of epoxy glue			Note
	Sieving pan, NO	Gran Size (mm)	Glue to Grain Percentage	
SS1	80	< 0.18	950 ml to 8.025 kg	
SS2	60+80	(0.25-0.425) +0.18	850 ml to 8.025 kg	Mix of 60 and 80
SS3	60	0.25- 0.425	850 ml to 8.025 kg	
SS4	40	0.425 - 0.85	750 ml to 8.025 kg	

B. Methods for determining index properties

1) *MIP Measurements:* As mentioned previously, mercury intrusion porosimetry (MIP) can be used to obtain a variety of parameters, such as permeability, porosity, median pore diameter, average pore diameter, and bulk density. The porosimeter uses a specialized pressure chamber as a means to force the mercury to fill porous substrate voids. Being forced by pressure, the mercury intrudes larger pores and then, under increasing pressure, starts intruding smaller pores. Using this approach, it is possible to characterize both intra- and inter-particle pores.

MIP utilizes the Washburn Equation to find the relation of applied pressure and pore diameter, applying the mercury’s physical characteristics [11]. These main characteristics are surface tension and the contact angle between the material and the mercury. In the Particle Technology Labs (PTL), various instrumentation and equipment are used that enable work to be carried out requiring pressures between around 1 psi and 60,000 psi. This range correlates well with pore measurements of between approximately 250 μm and 0.003 μm (3 nm).

Another consideration is the suitability of the mercury’s contact angle in relation to material being tested. If the contact angle cannot be measured or otherwise provided, default values are given for analysis. How much mercury enters the sample is monitored, by volume, using a penetrometer. A section of the penetrometer holds the sample. In this case, the sample size must be around 1.5 cm wide and 2.5 cm long. The MIP tests in the present study are conducted using a fine-grain sample and four synthetic sandstone samples. Throughout the course of the tests, pressure analyses are carried out. The results of the pressure testing show that the lowest and highest pressures are, respectively, 1 psia and 60,000 Psia. These readings relate well with the largest and smallest pore-throat diameters, respectively.

2) *Scanning Electron Microscopy:* As mentioned earlier, data related to pore throat size distribution is typically found by employing a mercury intrusion porosimetry. When this option is not available or unsuitable, we can use scanning electron microscope (SEM) images instead. SEM is able to examine microstructural pore characteristics at a nanoscale, so that the distribution, morphology and various types of

nanopores can be explored and determined. Nanoscale images for one fine-grain and four synthetic sandstone samples are taken using SEM. Prior to launching the imaging procedure, a surface from every sample of rock type is perpendicularly broken. The rock samples are 15 mm long, 5 mm high and 10 mm wide. The perpendicular breakage of the rock samples results in undamaged surfacing that reveals each sample’s pore structure. As a final step, the samples are digitally imaged using through-the-lens detector (TLD) mode.

II. RESULTS AND DISCUSSIONS

A. *MIP Measurements*

In testing for permeability, measurements for the fine-grain sample indicated a low permeability value of only 6.4133 mD, whereas the measurements for the four synthetic sandstone samples indicated high values (between 2035.9545 and 26151.7250 mD). In testing for porosity, the measurement results given for the synthetic samples using MIP indicated relatively large porosity compared to the real fine-grain sample. We can describe pore structure properties (e.g., amount and size) quantitatively by employing parameter sets derived from the MIP experiments. Table 2 shows the pore structure parameters for the investigated samples obtained from MIP. These parameters include permeability, porosity, tortuosity, median pore diameter.

TABLE 2. PARAMETERS OF PORE-SYSTEM STRUCTURE MEASURED BY MIP.

Sample name	The index properties for the samples			
	Permeability (mD)	Porosity (%)	Tortuosity	Median pore diameter (μm)
SR	6.5965	13.092	18.3575	0.0403
SS1	2035.954	33.3	3.19	32.14
SS2	6292.662	26.22	2.27	60.6101
SS3	8127.038	25.6	2.1	81
SS4	26151.72	25	1.7765	181.7485

How well a reservoir formation can store hydrocarbons is in large part determined by the reservoir rock’s porosity. Because porosity is such a key index characteristic, the accuracy of its characterization in relation to sandstone’s textural properties is highly beneficial. For sandstone, porosity represents the ratio of void volume (between the grains) to total rock volume. Compared to other rocks, sandstone generally has a broad porosity range. We found in our conducted tests that porosity (n) in the four synthetic sandstone samples ranged between 25% and 33%, for an average value of around 28%. Natural sandstone, on the other hand, typically has a porosity of 10% to 25%. If we plot the porosity and tortuosity from our test results against median grain size particles, we can see that synthetic fine-grained samples show higher porosity compared to coarse-grained samples (see Fig. 3). A clear relationship emerges showing porosity reduction in response to median grain size increases, and the results of tortuosity show the similar trend with median

grain size. The results also reveals that this relationship is not linear. These test results agree those found in previous studies, where porosity showed a reduction when grain sizes increased.

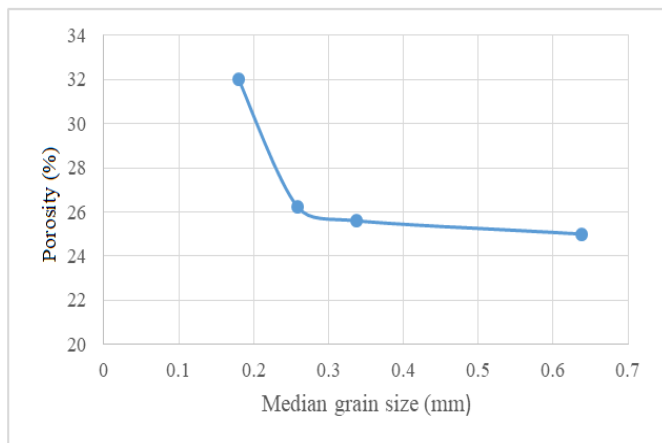


Fig. 3. EFFECT OF MEDIAN GRAIN SIZE ON POROSITY.

Conversely, mixing two-grain size ranges indicated a different trend, where both the permeability and porosity for the synthetic sandstone was reduced. The primary cause leading to the reduction in porosity is that smaller particles intruded the larger size voids. Porosity generally depends on the size of particles when there are uniform spheres and fixed bulk volumes (i.e., ideal system). However, a real system features different-sized particles, in which case the smaller particles cause a decrease in porosity by intruding any empty space between large particles. Hence, we can see from this that particle size, to a very great extent, determines porosity. Furthermore, the results reveal that systems which contain uniform particles (ideal systems) show that particle size and porosity are intimately related. This can be seen in cases SS1, SS3 and SS4. In the fine-grain sample (SR), however, where there are different-sized particles, porosity is reduced because of the smaller particles intruding on porous space. Another factor that decreased porosity in the fine-grain sample is the including of different grain sizes, as well as cementation and compaction. The empty spaces were intruded by cementitious materials, reducing the pore percentage for the solid sample. Important factor tested for in our experiments was permeability, which is the capacity for fluid in rock pores to move through reservoir rock. Permeability is directly related to the sample’s particle size as well as to its cementation and consolidation. In general, permeability is reduced when a solid features pores that are interconnected. This is because the empty spaces are intruded by smaller particles, in addition to cementation and compaction. Hence, in our tests, one sample (SS2) using two distinct sand sizes were mixed in order to appropriately represent a real reservoir environment. A rock’s dry bulk density can be defined as mass per unit volume. This parameter is highly affected by both the amount of pore space between grains and grain composition: more pore space leads to reduced density.

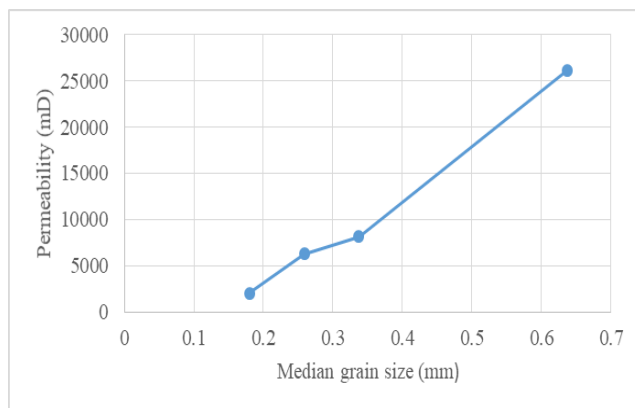


Fig. 4. EFFECT OF MEDAIN GRAIN SIZE ON PERMEABILITY.

Furthermore, because grain size impacts pore space, grain size likewise affects permeability and density. Figs. 4, 5 illustrate the test samples’ interrelationships of permeability and median pore diameter vs. median grain size, clearly indicating a direct relationship caused by reduced pore space due to increased grain size.

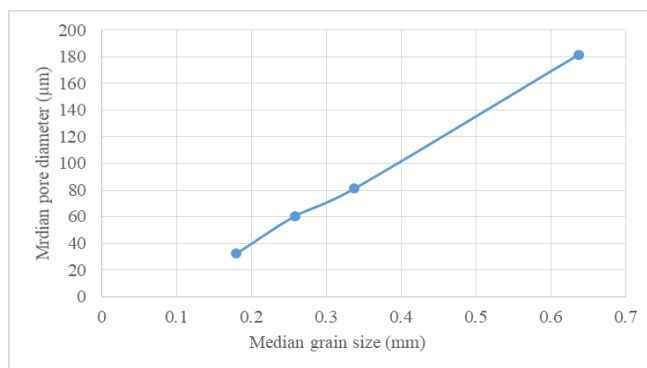


Fig. 5. RELATIONSHIP BETWEEN MEDIAN GRAIN SIZE AND MEDIAN PORE DIAMETER.

Using MIP experimental data, Figs. 6, 7 show the pore size distributions (PSD) curves as pore throat diameter vs. $dV/d\log D$ pore volume for both the fine-grain sample and the synthetic sandstone samples. As can be seen, the samples for both fine-grain and synthetic sandstone reveal PSD curves with single-peak distribution. Moreover, pore sizes are mainly in the range of 0.003 to 350 µm. In [16], Loucks et al. reported pore size classification schemes for fine-grain samples. In referring to their work, we can see that the dominant pores showing for our fine-grain sample can be classified as micropore ($1 \mu\text{m} \leq d < 62.5 \mu\text{m}$) with a 10 µm pore size. Also using [16] as a reference, the PSD curves of the four synthetic sandstone samples in our study show single peaks, which means that the synthetic sandstone samples have homogenies pore size distributions.

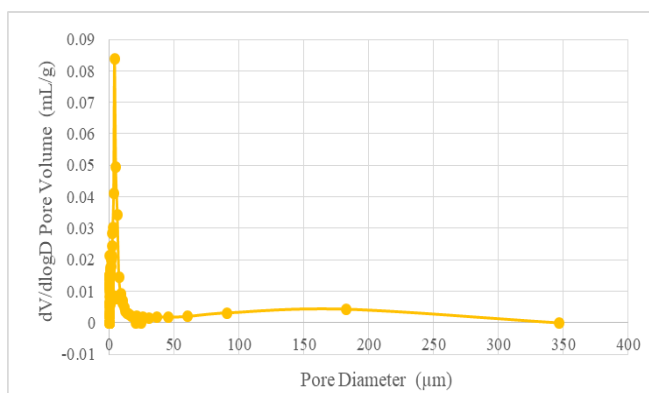


Fig. 6. PORE SIZE DISTRIBUTION (PSD) CURVES OF FINE-GRAIN SANDSTONE SAMPLE.

Fig. 7 shows PSD curves from synthetic samples of differently sized grains (i.e., SS1, SS2, SS3 and SS4) as measured with MIP. As can be seen, there is a rise in cumulative porosity in samples of the same grain size as well as those for mixing grain size samples. Although this increase is not significant in pore throat sizes below 30 μm, most of the pores from the synthetic sandstone samples are 30 μm or larger and feature pore size distribution that is homogenies. In any case, the figs. 6, 7 show a PSD curve trend similarity between the fine-grain sandstone sample (SR) and the synthetic sandstone samples (SS1, SS2, SS3 and SS4), other than for variations in the pore size due to the samples' differently sized grains.

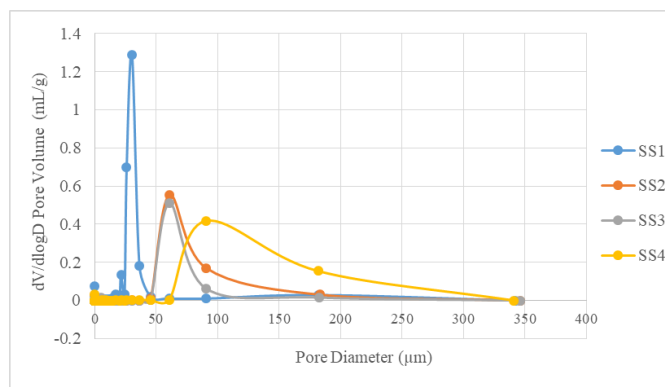


Fig. 7. PORE SIZE DISTRIBUTION (PSD) CURVES OF THE FOUR SYNTHETIC SANDSTONE SAMPLES.

B. SEM Measurements

By investigating and analyzing pore structure, we can better understand the fluid transport mechanism in sandstone. We proposed a quantitative approach for characterizing the distribution of pore sizes in synthetic sandstone and fine-grain sandstone samples, using scanning electron microscopy (SEM). Following an initial SEM scan, we chose specific SEM images we considered representative among dozens of images. The

main aim was to best showcase the samples' micro-morphology. As SEM image magnification can affect the quality and type of information it relays, choosing appropriate magnification parameters is crucial. Following several attempts to obtain accurate representations of the needed data. We chose SEM image from the identical scanned area and from the identical operating voltage (30 kV), but showing different magnifications. These differences in magnification revealed the images' meso-morphology features for the samples, as depicted by Figs. 8, 9.

Having chosen these SEM images, we could clearly observe the pores, grains and glue content, along with the material and structural morphology for the samples. SEM imagery was then employed qualitatively in order to characterize the samples' pore sizes. Fig. 9 depicts the original SEM image as a greyscale picture (predominantly grey and black), with the grey portions indicating grain matrix and the black portion possibly denoting the pore. In addition, the transition zone (black to white) could indicate an interface existing between the grain matrix and the pore.

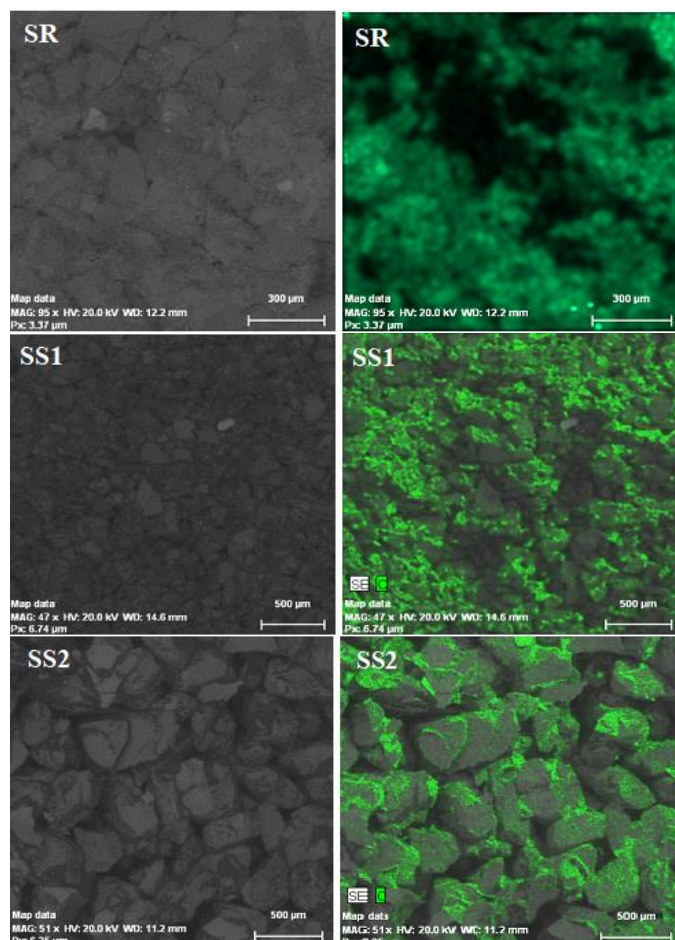


Fig. 8. THE SEM IMAGES OF SYNTHETIC SANDSTONE (SS1 AND SS2) AND FINE-GRAIN SANDSTONE SAMPLES.

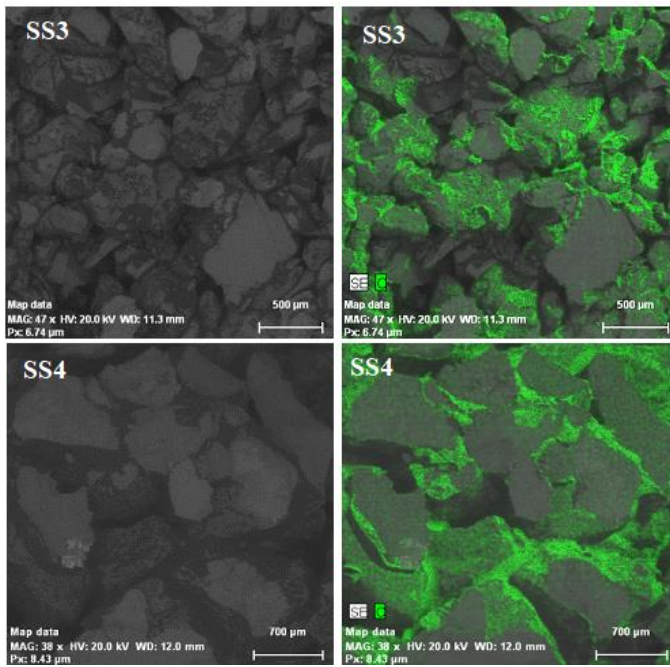


Fig. 9. THE SEM IMAGES OF SYNTHETIC SANDSTONE SAMPLES (SS3 and SS4)

As well, the green map images reveal the distribution of epoxy glue content between the grains. From the map, we can see SEM images showing how reductions of grain sizes require additional epoxy glue content because the smaller the grain size, the more glue is needed. As depicted, the glue located at the contact area of the grain. It creates binder bonds which grow harder and join sand particles when sintered. Hence, as the amount of bonds and extensions increases, so does the glue. During this process, particles become involved, intruding empty spaces and causing decreases in permeability and porosity. The SEM imagery ultimately indicated similar pore size distribution, similar pore orientation, similar pore shape and similar microstructure, all of which points to the porosity and mineralogy in the six artificial samples being homogeneous. Finally, we saw that areas within the SEM imagery showed connecting pore throats among the pores in the sandstone matrix. As revealed in Fig. 9, the pore throats exhibited nearly the same diameters, indicating that pores can be characterized as pervasive in addition to being interconnected with the glue matrix.

Conclusion

This paper presents a technique for preparing homogenised synthetic sandstone samples that can be applied in the hydrocarbon recovery projects. The mercury intrusion porosimetry (MIP) and scanning electron microscopy (SEM) have been used to first characterize and then analyze the pore morphology and index properties for the synthetic sandstone samples. The following conclusions can be summarized:

- A. The experimental results indicated that weak solidified sandstone index characteristics are strongly affected by both mixing and grain size.
 - 1) The results exhibited an inverse relation between the samples' porosity and the grain size, with porosity experiencing a non-linear reduction with increases in grain size.
 - 2) The results also showed direct relationships between grain size and other properties such as permeability and median pore diameter. In this case, permeability levels rose with increases in median grain size. This tendency appears to have an indirect relation with reductions in porosity, considering median grain size as a function.
 - 3) The results point to reductions in both permeability and porosity when two different grain sizes are mixed. The primary cause for the initial reduction in permeability and porosity appears to be the infilling of larger-sized voids with smaller-sized particles.
 - 4) The PSD curves showed homogenous pore size distributions and trend similarity between the fine-grain sandstone sample and the synthetic sandstone samples.
- B. Furthermore, SEM map images revealing pore morphologies and grain distribution of the tested samples indicate that grains that undergo reductions in size require additional epoxy glue content, likely due to binder distribution of glue among the small grains.

REFERENCES

- [1] O. R. Cardoso and R. D. C. Balaban, "Comparative study between Botucatu and Berea sandstone properties," *J. South Am. Earth Sci.*, vol. 62, pp. 58–69, 2015.
- [2] L. C. Marques, C. R. Appoloni, C. P. Fernandes, "Porosity Study of Synthetic Sandstones by Non-Destructive Nuclear Techniques," vol. 14, no. 3, pp. 394–402, 2011.
- [3] V. Fattahpour, B. Anne, and M. Moosavi, "Effect of grain characteristics and cement content on the unconfined compressive strength of artificial sandstones," *International Journal of Rock Mechanics & Mining Sciences.*, vol. 72, pp. 109–116, 2014.
- [4] Q. Xiong, T. G. Baychev, and A. P. Jivkov, "Review of pore network modelling of porous media: Experimental characterisations, network constructions and applications to reactive transport," *J. Contam. Hydrol.*, vol. 192, pp. 101–117, 2016.
- [5] R. Yang, S. He, J. Yi, and Q. Hu, "Nano-scale pore structure and fractal dimension of organic-rich Wufeng-Longmaxi shale from Jiaoshiba area, Sichuan Basin: Investigations using FE-SEM, gas adsorption

- and helium pycnometry,” *Mar. Pet. Geol.*, vol. 70, pp. 27–45, 2016.
- [6] M. Sun, B. Yu, Q. Hu, S. Chen, W. Xia, and R. Ye, “Nanoscale pore characteristics of the Lower Cambrian Niutitang Formation Shale: A case study from Well Yuke # 1 in the Southeast of Chongqing, China,” *Int. J. Coal Geol.*, vol. 154–155, pp. 16–29, 2016.
- [7] R. G. Loucks, R. M. Reed, S. C. Ruppel, and U. Hammes, “Spectrum of pore types and networks in mudrocks and a descriptive classification for matrix-related mudrock pores,” vol. 6, no. 6, pp. 1071–1098, 2012.
- [8] J. Klaver, G. Desbois, J. L. Urai, and R. Littke, “BIB-SEM study of the pore space morphology in early mature Posidonia Shale from the Hils area, Germany,” *Int. J. Coal Geol.*, vol. 103, pp. 12–25, 2012.
- [9] K. Jiao *et al.*, “The characterization and quantitative analysis of nanopores in unconventional gas reservoirs utilizing FESEM – FIB and image processing: An example from the lower Silurian Longmaxi Shale, upper Yangtze region, China,” *Int. J. Coal Geol.*, vol. 128–129, pp. 1–11, 2014.
- [10] S. Zhou, G. Yan, H. Xue, and W. Guo, “2D and 3D nanopore characterization of gas shale in Longmaxi formation based on FIB-SEM,” *Mar. Pet. Geol.*, vol. 73, pp. 174–180, 2016.
- [11] H. Giesche, “Mercury Porosimetry: A General (Practical) Overview,” vol. 23, no. September 2005, pp. 9–19, 2006.
- [12] C. Vavra, N. Star, G. Services, and J. Kaldi, “Geological applications of capillary pressure: A review,” no. May, 2015.
- [13] N. Zhang, M. He, B. Zhang, F. Qiao, H. Sheng, and Q. Hu, “Pore Structure Characteristics and Permeability of Deep Sedimentary Rocks Determined by Mercury Intrusion Porosimetry,” vol. 27, no. 4, pp. 670–676, 2016.
- [14] R. Yang, F. Hao, S. He, C. He, X. Guo, and J. Yi, “Experimental investigations on the geometry and connectivity of pore space in organic-rich Wufeng and Longmaxi shales,” *Mar. Pet. Geol.*, vol. 84, pp. 225–242, 2017.
- [15] J. Lai and G. Wang, “Fractal analysis of tight gas sandstones using high-pressure mercury intrusion techniques,” *Journal of Natural Gas Science and Engineering*, vol. 24, pp. 185–196, 2015.
- [16] R. G. Loucks, R. M. Reed, S. C. Ruppel, and U. Hammes, “Spectrum of pore types and networks in mudrocks and a descriptive classification for matrix-related mudrock pores,” *AAPG Bulletin*, vol. 96, no. 6, pp. 1071–1098, 2012.